Spatial Modelling of the Terrestrial Environment

Editors

RICHARD E.J. KELLY

Goddard Earth Science and Technology Center, University of Maryland

NICHOLAS A. DRAKE

Department of Geography, Kings College London

STUART L. BARR

School of Geography, University of Leeds

John Wiley & Sons, Ltd

7

Modelling Wind Erosion and Dust Emission on Vegetated Surfaces

Gregory S. Okin and Dale A. Gillette

7.1 Introduction

Erosion, transportation and deposition of material by wind are fundamental abiotic processes in the world's drylands. Atmospheric dust created in deserts by wind erosion and subsequently transported around the globe is a vital component of the entire Earth system. Mineral particulates from local or regional sources can dramatically impact air quality. Despite this, there is often little information about where, precisely, in the landscape wind erosion and dust emission occur. This is largely because the conditions on the surface that determine the extent and degree of wind erosion tend to vary across both space and time and relatively complex interactions between soil and vegetation conspire to allow or suppress wind erosion. Although the mathematical understanding of wind erosion and dust emission has progressed to a point where current models can accommodate a fair degree of complexity, few studies to date have integrated the models in such a way that spatially explicit estimates of wind erosion and dust flux can be made. This technological step is required if we are to start to understand the distribution of atmospheric dust observed from remote sensing platforms or are to predict dust events that can affect local human health or global biogeochemical cycles.

The purpose of the present research is to develop a modelling framework in which spatially explicit estimates of wind erosion and dust emission for vegetated surfaces can be derived. The model that is developed here allows land surface-based estimates of dust emission at the regional scale and is intended to be complementary to global scale estimates of dust emission that can be derived from modelling (e.g. Tegen *et al.*, 1996). Coarse resolution remote sensing observations of the atmosphere using sensors such as the Total

Spatial Modelling of the Terrestrial Environment. Edited by R. Kelly, N. Drake, S. Barr.
 ISBN: 0-470-84348-9.

Ozone Mapping Spectrometer (TOMS) (e.g. Prospero, 1999) and meteorological satellites such as METEOSAT (Legrand *et al.*, 1989) also provide useful general information on source areas. While global scale estimates of atmospheric dust distributions are routinely produced using these sensors, land surface-based wind erosion estimation remains in its infancy, particularly when applied at the regional scale. This chapter is intended to describe the state of the science of regional scale modelling, outline the implementation of a regional scale model and identify future areas for research.

7.1.1 The Importance of Atmospheric Dust

Atmospheric mineral dust can affect the global energy balance by changing the radiative forcing of the atmosphere through its ability to scatter and absorb light (Sokolik and Toon, 1996; Tegen and Lacis, 1996). Atmospheric mineral aerosols may also provide surfaces for reactions, change the concentration of other aerosols in the atmosphere and affect cloud nucleation and optical properties (Dentener *et al.*, 1996; Levin *et al.*, 1996; Dickerson *et al.*, 1997; Wurzler *et al.*, 2000). The iron in dust is thought to play a major role in ocean fertilization and oceanic CO_2 uptake-thereby affecting the global carbon budget (Duce and Tindale, 1991; Coale *et al.*, 1996; Piketh *et al.*, 2000). Dust transported to downwind terrestrial ecosystems can play a major role in soil formation and nutrient cycling (Chadwick *et al.*, 1999; Reynolds *et al.*, 2001) and present serious health concerns (Griffin *et al.*, 2001).

On local and regional scales, anthropogenic disturbance can have consequences on wind erosion and plant community composition and nutrient cycling in arid and semiarid environments. Human land use practices can reduce vegetation cover and expose wind-erodible soils to mobilization (Stockton and Gillette, 1990; Tegen and Fung, 1995; Lancaster and Baas, 1998; Okin *et al.*, 2001a). For example, the Dust Bowl resulted from a decade-scale drought and poor land use practices and showed that throughout the central United States, wind erosion remains a potentially important ecosystem and geomorphic process (Schlesinger *et al.*, 1990; Forman *et al.*, 1992; Rosenzweig and Hillel, 1993; Schultz and Ostler, 1993; Brown *et al.*, 1997; Alward *et al.*, 1999).

Recent results from the Jornada Basin in south-central New Mexico, part of the National Science Foundation's Long-Term Ecological Research (LTER) network, indicate that severe wind erosion can induce both plant community change and disruption of the soil nutrient cycle (Okin *et al.*, 2001b). A site was cleared of vegetation in 1990 for an experiment aimed at measuring dust flux from the loamy sand soils common at Jornada (Figure 7.1). In the 11 years since its establishment, the site and the area directly downwind of it have undergone major changes in nutrient budget and community composition (Okin *et al.*, 2001b). Here, removal of vegetation has triggered wind erosion by enhancing particle saltation and suspension processes. Saltation of sand-sized grains leads to negative physical consequences for vegetation such as burial and abrasion. Since plant nutrients are concentrated on suspension-sized particles, suspension leads to the permanent removal of nearly all soil nutrients in the surface soils in approximately 10 years. Thus, saltation kills mature vegetation while suspension inhibits the growth of new plants, leading to changes in plant community by differentially affecting shrub and grass species. With their biomass largely below the saltation layer, grasses are abraded and buried by sand particles, whereas shrubs are largely spared this fate. Growth of new plants (including annuals) that rely on nutrients

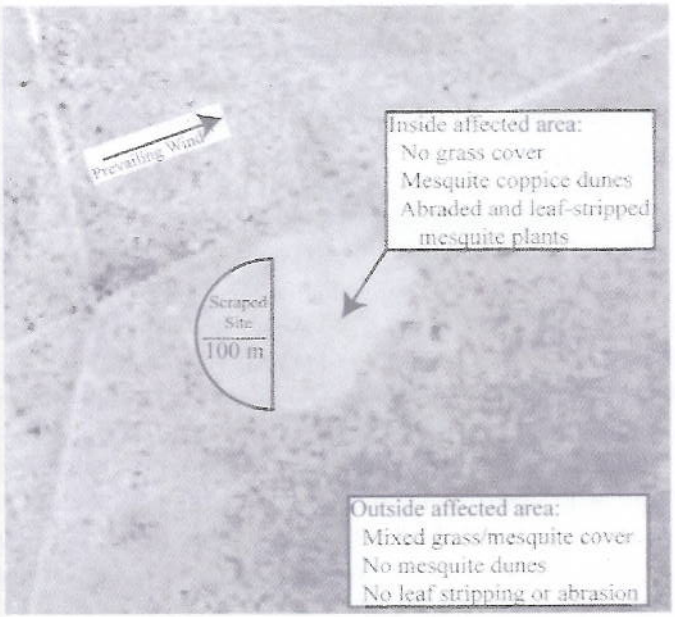

Figure 7.1 *The Jornada 'scraped site' shown here in a 1999 low-altitude airborne visible/infrared spectroradiometer (AVIRIS) image with resolution of ~5 m. This site proves that wind erosion can affect ecosystem stability in this ecosystem. It has experienced an average deflation rate of 1.8 cm* yr^{-1} *(Gillette and Chen, 2001) and plant-available N and P have been reduced by 89% and 78%, respectively (Okin et al., 2001b). No vegetation has regrown on the scraped site itself. The vegetation community downwind of the site has changed from a grassland to a shrubland due to burial, abrasion and leaf stripping from saltating particles from the scraped site itself (Okin et al., 2001a) and plant-available N and P in surface soils in the downwind area have been reduced by 82% and 62%, respectively (Okin et al., 2001b)*

in the topmost soil layer is inhibited. The seedbank may also be depleted in the winnowed surface soils (A. van Rooyen, personal communication). Thus perennial grasses are killed, new vegetation growth is suppressed and shrubs, where established, gain a competitive edge. Creation of an erosive discontinuity in a mixed shrub/grass ecosystem accelerates the conversion of grassland to shrubland.

7.1.2 Where Does the Dust Come from?

Despite the importance of desert dust, it is often unclear in detail where it is produced and what role humans play in mediating its production. Sensors such as TOMS can be used to directly observe dust in the atmosphere using methods such as the TOMS aerosol index (e.g. Prospero, 1999), but current technologies do not allow unique identification of the loci due to their coarse resolution and, in the case of TOMS, because of problems in observing the lower levels of the atmosphere. Because of this, controversy remains about the extent to which land use contributes to the atmospheric mineral dust. Recent work by Prospero *et al.* (2002) and Ginoux *et al.* (2001) suggests that the overwhelming majority of desert dust comes from closed basins in arid areas related to now-dry or ephemeral lakes. They argue further that humans do not significantly perturb the dust cycle, a conclusion supported by

Guelle *et al.* (2000). This point of view contrasts sharply with that of Tegen and Fung (1995) who suggest that land use may in fact dramatically affect the amount of dust emitted in desert regions.

7.1.3 Aims and Objectives

In summary, all of the studies which have examined dust emission in order to disentangle the natural and land use signals have either used coarse scale modelling or remote sensing data where there are many potential sources in each pixel that could produce the observed atmospheric distribution. In order to resolve the question of the contribution of land use and land cover to desert dust, local or regional scale models that incorporate data from the Earth's land surface are required to identify dust sources. But dust emission depends on several soil and vegetation parameters (e.g. soil texture, crown height and plant density) that can vary in both space and time. New techniques which allow modelling of wind erosion and dust emission based on known distributions of vegetation and soils in small well-studied areas are a necessary first step in achieving the goal of land surface-based models of wind erosion. The aim of the present chapter is to do just this for the Jornada Basin in south-central New Mexico.

7.2 Study Site Description

The Jornada del Muerto basin lies approximately 30 km northeast of Las Cruces, NM, in the Chihuahuan Desert ecosystem (Figure 7.2). It is bounded by the San Andres mountains on the east and by the Rio Grande valley and the Fra Cristobal-Caballo mountain complex on the west. Elevation above sea level varies from 1180 to 1360 m. The Jornada Plain consists

Figure 7.2 Location of the Jornada Basin, New Mexico. Maps from National Atlas of the United States, October 29, 2003, www.nationalatlas.gov

of unconsolidated Pleistocene detritus. This alluvial fill from the nearby mountains is 100 m thick in places and the aggradation process is still active. Coarser materials are found near foothills along the eastern part of the study area. The topography of the study area consists of gently rolling to nearly level uplands, interspersed with swales and old lakebeds (Buffington and Herbel, 1965).

The climate of the area is characterized by cold winters and hot summers and displays a bimodal precipitation distribution. Winter precipitation usually occurs as low-intensity rains or occasionally as snow and contributes to the greening of shrub species in the basin in the early spring. Summer monsoonal precipitation, usually in the form of patchy, but intense, afternoon thunderstorms, is responsible for the late-summer greening of grasses. The average annual precipitation between 1915 and 1962 in the basin was 230 mm, with 52% falling between July 1 and September 30 (Paulsen and Ares, 1962). The average maximum temperature is highest in June, when it averages 36°C and lowest in January, when it averages 13°C (Buffington and Herbel, 1965).

The principal grass species in the study area are *Scleropogon brevifolius* (burrograss), *Hilaria mutica* (tobosa grass) and several species of *Aristida* while major shrubs are *Larrea tridentata*, *Prosopis glandulosa*, and *Florensia cernua*. Soils in the basin are quite complex but generally range from clay loams to loamy fine sands, with some areas being sandy or gravelly (Soil Conservation Service, 1980).

The Jornada Basin is an area of intense research as part of the Jornada LTER programme of the National Science Foundation. The primary reason for the broad scientific interest in the Jornada Basin is because it is the premier site in which widespread conversion of grassland communities to shrublands over the past 100 years (Buffington and Herbel, 1965; Bahre, 1991) has been studied. Grazing and other anthropogenic disturbances are commonly invoked to explain this trend (Bahre and Shelton, 1993). Extensive work on soil structure and plant community composition at the Jornada LTER site and the adjacent New Mexico State University (NMSU) Ranch strongly supports this hypothesis (Schlesinger *et al.*, 1990).

7.3 Review of Basic Equations Relating to Wind Erosion Modelling

Saltation mass flux has been related by a large number of authors using different approaches. Bagnold (1941) approached the problem first and provided a physically reasonable solution that was later confirmed by the analysis of Owen (1964). The saltation equation has been verified by wind tunnels, field experiments and alternate theoretical derivations (Shao and Raupach, 1993):

$$Q_{\mathrm{Tot}} = A\frac{\rho}{g}\sum_{u_*} u_*\left(u_*^2 - u_{*t}^2\right)\Delta T, \tag{1}$$

where Q_{Tot} is the horizontal (saltation) mass flux (g cm^{-1} s^{-1}), A is a unitless parameter (usually assumed to be equal to 1) related to supply limitation (Gillette and Chen, 2001), ρ is the density of air (g cm^{-3}), g is the acceleration of gravity (cm s^{-1}), u_* is the wind shear velocity and u_{*t} is the threshold shear velocity (both cm s^{-1}). Q_{Tot} is envisioned as the mass flowing past a pane one length unit wide, perpendicular to both the wind and the ground. Vertical mass flux (dust flux), F_a (g cm^{-2} s^{-1}), is linearly related to Q_{Tot} by a constant K

Table 7.1 *Variations in F_a/Q_{tot} as a function of soil texture (from Gillette et al. (1997))*

Texture	Log of F_a/Q_{tot}(cm^{-1})			Number of samples
	Average	Minimum	Maximum	
Clay	−6.4	−6.5	−6.3	2
Loam	−5.7	−5.7	−5.7	1
Sandy loam	−3.7	−4.1	−3.5	2
Loamy sand	−4.5	−5.9	−4.2	7
Sand	−5.7	−6.6	−5.1	28

(cm^{-1}) that is typically of order of 10^{-4}–10^{-5} cm^{-1} that varies with soil texture (see Table 7.1) (Gillette *et al.*, 1997). F_a is envisioned as the mass leaving the surface per unit time.

The shear velocities, u_* and u_{*t}, are related to wind speed at height z, $U(z)$ (cm s^{-1}), by:

$$U(z) = \frac{u_*}{k} \ln\left(\frac{z - D}{z_0}\right). \tag{2}$$

where k is von Karmann's constant (unitless), z_0 is the roughness height (cm) and D is the displacement height (cm). If $D > 0$, then turbulent flow in wakes predominates and no wind erosion can occur.

Kaimal and Finnigan (1994, p. 68) have suggested that D is approximately related to canopy height, h_c (cm) by:

$$D = 0.75h_c. \tag{3}$$

While this relationship may hold when considering boundary layer phenomena that take place above the canopy, equation (3) dictates a non-zero D and therefore no wind erosion, for all vegetated surfaces (surfaces with $h_c \neq 0$). Modelling approaches to wind erosion must assume that $D = 0$, so that wind erosion is allowed on vegetated surfaces and roughness height, z_0, must be assumed to be the determinant of the relationship between $U(z)$ and u_*.

Several authors have proposed relations to predict z_0 as a function of surface roughness. Lettau (1969) and Wooding *et al.* (1973) have suggested parameterization of z_0 by:

$$z_0 = 0.5h_c\lambda, \tag{4}$$

where λ is a unitless parameter known as 'lateral cover' (Raupach *et al.*, 1993) or 'roughness density' (Marticorena *et al.*, 1997). Lateral cover is equal to the average frontal area of plants multiplied by their number density, N (cm^{-2}). Number density is related to fractional cover of vegetation, C (unitless) by:

$$N = \frac{C}{A_p}, \tag{5}$$

where A_p is the average footprint of individual plants (cm^2).

The linear relation in equation (4) should hold until λ reaches ~0.1. Above this value, z_0/h_c remains approximately constant. Marticorena *et al.* (1997) have adjusted equation (4) to incorporate the levelling-off of the linear relationship with increasing λ:

$$z_0 = \begin{cases} (0.479\lambda - 0.001)h_c & \text{for } \lambda \leq 0.11 \\ 0.005h_c & \text{for } \lambda > 0.11 \end{cases} \quad (6)$$

Thus, using either equation (4) or (6), one can predict z_0 based on knowledge of vegetation parameters and assuming randomly distributed vegetation.

For conditions of partial, randomly distributed vegetation cover, u_{*t} is related to the threshold shear velocity for an unvegetated surface u_{*ts} by:

$$u_{*t} = u_{*ts}\sqrt{(1 - \sigma\lambda)(1 + \beta\lambda)}, \quad (7)$$

where σ (unitless) is equal to the ratio of the average basal area to average frontal area of individual plants, β (unitless) is the ratio of the drag coefficient of an isolated plant to the drag coefficient of the ground surface in the absence of the plant and is of order 10^2.

The wind erosion and dust flux model discussed above (equations (1)–(3)) assumes randomly and isotropically spaced vegetation. In desert areas, particularly in areas undergoing severe wind erosion, this may not be the case. Okin and Gillette (2001) have shown using standard geostatistical techniques and 1-m resolution digital orthophotos that vegetation can be distributed anisotropically which can enhance dust emission. They found that in mesquite dunelands in the northern Chihuahuan Desert, vegetation is oriented in elongated areas whose direction nearly parallels the direction of the prevailing wind. These landscapes also display horizontal mass fluxes (Q_{Tot}) several times those observed in adjacent lands dominated by other vegetation. The vegetation-free areas elongated in the direction of the dominant eroding winds that accounted for the increased wind erosion were named 'streets'. It is likely that the streets are the primary loci of wind erosion and that in areas without streets, or at times when the wind is not aligned with the streets, the wind erosion from the area is negligible.

7.4 The Spatially Explicit Wind Erosion and Dust Flux Model

Significant work over the past half-century has led to the development of parameterized wind erosion models that are based on theoretical consideration, field experiments and wind-tunnel experiments. A small number of parameters controls wind erosion and dust flux in areas with randomly distributed partial cover. The model parameters, in turn, are closely related to characteristics of the soil (e.g. surface texture) and vegetation (e.g. crown size and geometry, plant number density, plant distribution anisotropy) (Table 7.2).

In the present research, we have created a spatially explicit wind erosion and dust flux model (SWEMO) that allows estimation of wind erosion and dust flux across a landscape by incorporating spatial distributions of important parameters. Users can thus see how in the landscape soil and vegetation parameters interact to create patterns of wind erosion and dust emission. This approach provides a powerful basis for trying to understand where in landscapes the strongest dust sources are and is therefore applicable to trying to understand the most important or persistent dust sources in an area. At its heart are flux equations that represent the state of the art in wind erosion and dust flux modelling, discussed above,

The linear relation in equation (4) should hold until λ reaches ~0.1. Above this value, z_0/h_c remains approximately constant. Marticorena *et al.* (1997) have adjusted equation (4) to incorporate the levelling-off of the linear relationship with increasing λ:

$$z_0 = \begin{cases} (0.479\lambda - 0.001)\,h_c & \text{for} \quad \lambda \leq 0.11 \\ 0.005 h_c & \text{for} \quad \lambda > 0.11 \end{cases} \tag{6}$$

Thus, using either equation (4) or (6), one can predict z_0 based on knowledge of vegetation parameters and assuming randomly distributed vegetation.

For conditions of partial, randomly distributed vegetation cover, u_{*t} is related to the threshold shear velocity for an unvegetated surface u_{*ts} by:

$$u_{*t} = u_{*ts}\sqrt{(1 - \sigma\lambda)(1 + \beta\lambda)}, \tag{7}$$

where σ (unitless) is equal to the ratio of the average basal area to average frontal area of individual plants, β (unitless) is the ratio of the drag coefficient of an isolated plant to the drag coefficient of the ground surface in the absence of the plant and is of order 10^2.

The wind erosion and dust flux model discussed above (equations (1)–(3)) assumes randomly and isotropically spaced vegetation. In desert areas, particularly in areas undergoing severe wind erosion, this may not be the case. Okin and Gillette (2001) have shown using standard geostatistical techniques and 1-m resolution digital orthophotos that vegetation can be distributed anisotropically which can enhance dust emission. They found that in mesquite dunelands in the northern Chihuahuan Desert, vegetation is oriented in elongated areas whose direction nearly parallels the direction of the prevailing wind. These landscapes also display horizontal mass fluxes (Q_{To}) several times those observed in adjacent lands dominated by other vegetation. The vegetation-free areas elongated in the direction of the dominant eroding winds that accounted for the increased wind erosion were named 'streets'. It is likely that the streets are the primary loci of wind erosion and that in areas without streets, or at times when the wind is not aligned with the streets, the wind erosion from the area is negligible.

7.4 The Spatially Explicit Wind Erosion and Dust Flux Model

Significant work over the past half-century has led to the development of parameterized wind erosion models that are based on theoretical consideration, field experiments and wind-tunnel experiments. A small number of parameters controls wind erosion and dust flux in areas with randomly distributed partial cover. The model parameters, in turn, are closely related to characteristics of the soil (e.g. surface texture) and vegetation (e.g. crown size and geometry, plant number density, plant distribution anisotropy) (Table 7.2).

In the present research, we have created a spatially explicit wind erosion and dust flux model (SWEMO) that allows estimation of wind erosion and dust flux across a landscape by incorporating spatial distributions of important parameters. Users can thus see how in the landscape soil and vegetation parameters interact to create patterns of wind erosion and dust emission. This approach provides a powerful basis for trying to understand where in landscapes the strongest dust sources are and is therefore applicable to trying to understand the most important or persistent dust sources in an area. At its heart are flux equations that represent the state of the art in wind erosion and dust flux modelling, discussed above,

Table 7.2 Relations between wind erosion model parameters and vegetation/soil parameters

Model parameter		Vegetation/Soil parameter
Threshold shear velocity of soil	u_{*ts}	Soil grain size, crusting, disturbance
Displacement height	D	Assumed to be zero
Roughness height	z_0	Plant height, radius, and density
Basal/Frontal area ratio	σ	Plant height and radius
Drag coefficient ratio	β	Approx. constant (~100)
Lateral cover	λ	Plant height, radius and number density
Fractional cover	C	Plant radius and density
Number density	N	Fractional cover and plant radius

which are similar to those used by Marticorena *et al.* (1997) in their simulation of Saharan dust sources.

SWEMO uses maps of soil texture and vegetation, in addition to knowledge of vegetation cover and size parameters, to create derived maps of threshold shear velocity (with vegetation), u_{*t} and z_0. Values u_{*ts} are derived by extracting median values of u_{*ts} for each soil texture class from Gillette *et al.* (1997). Soil crusting and disturbance were not included in this version of the model. For each cell in the model, a histogram of shear velocity is derived from a histogram of wind speed at one height using the value of z_0 at that cell and equation (2). Equation (1) is then evaluated for each cell to derive an estimate of total horizontal flux, Q_{Tot}. A soil-texture based value of F_a/Q_{Tot} (see Table 7.1) is then used to calculate the amount of vertical flux, F_a, for each cell. The processing stream for SWEMO is depicted in Figure 7.3.

7.4.1 Issues in the Integration of Parameters for SWEMO

Wind erosion depends on several parameters that vary as a function of soil and vegetation cover. By using maps of dominant vegetation type and soil texture, SWEMO is able to impose spatial variability by allowing the main parameters that determine wind erosion and dust flux (see Table 7.3) to vary according to the specific soil and vegetation found at any location. Thus, the primary constraint on the use of SWEMO in natural landscapes is the availability of overlapping vegetation and soil maps that provide information at scales of interest.

However, even if categorical maps of soil texture and vegetation type, with polygons labelled, for example, 'sandy loam' and 'creosote', are 100% accurate, they do not represent the full variability of the landscape: among other things, the size and spacing of plants vary even among areas with the same polygon labels. Thus, although SWEMO is able to evaluate the wind erosion equations (equations (1) and (2)) using different parameters for different soils and community types, those parameters cannot vary in the model within classes. In addition, the parameters used to evaluate the wind erosion equations must be derived from literature values or field measurements and there is no guarantee that the values chosen for integration into SWEMO are representative over the entire area of interest.

Finally, and probably most important, the majority of wind erosion may occur in small areas not well represented by local averages. A small hole in vegetation, such as a natural

Table 7.3 *SWEMO input parameters for soils of the Jornada Basin*

Texture	Sandy loam	Loamy sand	Clay loam	Gravelly sand
u_{*ts} (cm s^{-1})	29	34	68	28
Log(F_a/Q_{tot} (cm^{-1}))	−3.7	−4.5	−5.7	−5.7
A	1.0	1.0	1.0	1.0

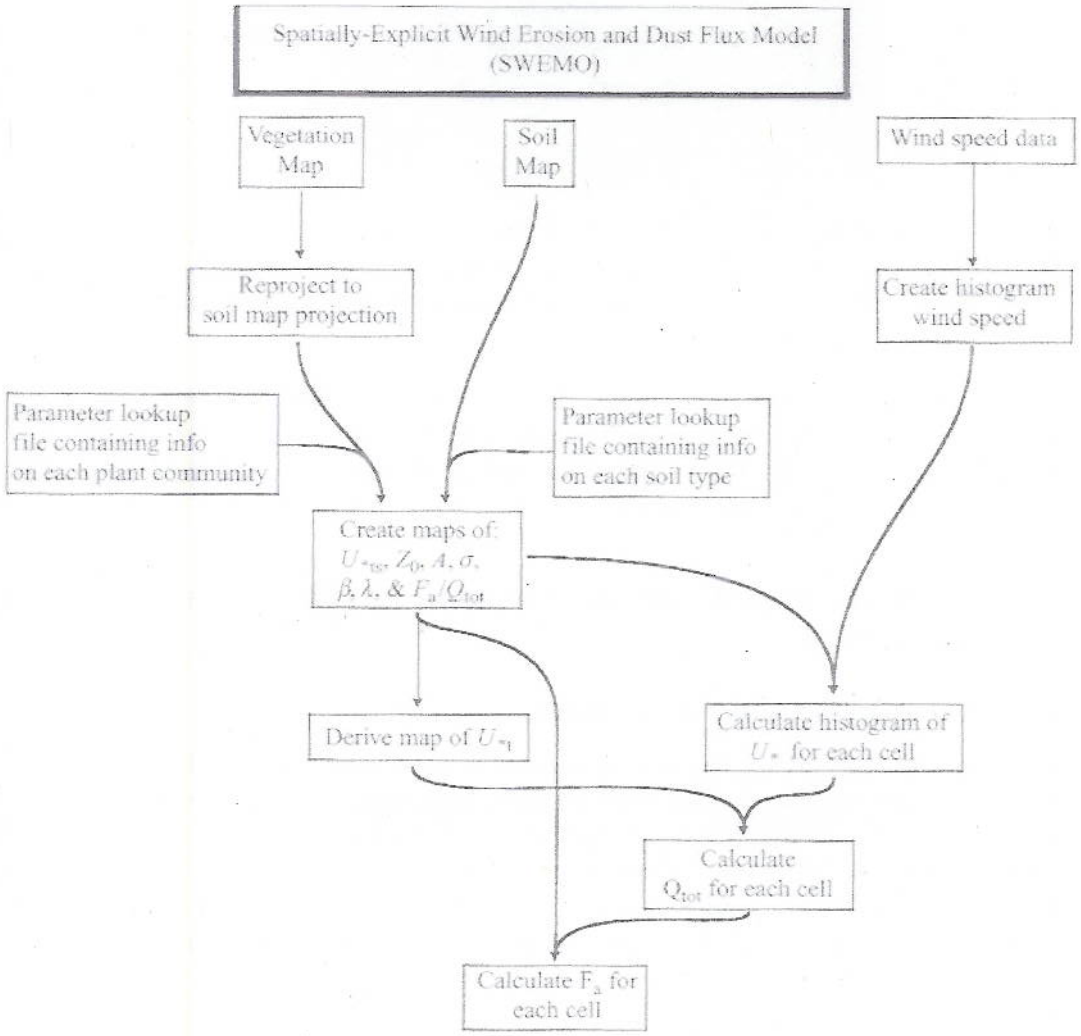

Figure 7.3 *Processing stream for the spatially explicit wind erosion and dust flux model (SWEMO).*

disturbance, a road, a dry river or a dry lake, may account for the majority of dust emitted in an area, but be insignificant on the scale at which most maps are produced.

In the present study, a site with all requisite data (soil maps, vegetation maps, wind data and a wealth of ongoing ecological research) was chosen to test SWEMO. The Jornada

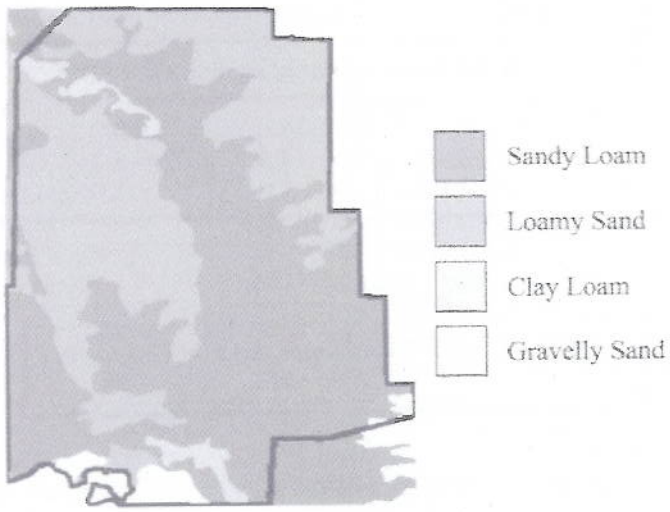

Figure 7.4 Soil texture map of the Jornada Basin derived from the soil survey of Doña Ana County, New Mexico (Soil Conservation Service, 1980). The area outlined in black is the region where the soil and vegetation maps overlap and is the study area for the present research

Basin in south-central New Mexico is a part of the National Science Foundation's LTER network and as such provides a wealth of required and ancillary data. Ongoing research into dust emissions at this site by one of the authors (Gillette) also allows us to compare modelled fluxes with measured values.

7.5 Using SWEMO to Predict Wind Erosion and Dust Flux at the Jornada Basin

7.5.1 Data Sources and Model Inputs

Soil Data. Portions of the Jornada Basin have been mapped by the US Soil Conservation Service (1980) (Figure 7.4). Each polygon in this soil map is labelled with a soil texture of the dominant soil type in that polygon, which allows estimation of u_{*ts} and F_a/Q_{Tot} (Table 7.3). The particle-limitation coefficient, A, is assumed to be 1.0 for the entire study area. Values of u_{*ts} used in this study were derived from mean values provided by Gillette (1988). Values of F_a/Q_{Tot} were estimated using data from Gillette *et al.* (1997) (see Table 7.2).

Vegetation Data. A vegetation map of portions of the Jornada Basin was made available to these study through the Jornada LTER project (digital data produced by R. Gibbens, R. McNeely and B. Nolen). This map contained information on spatial distribution of the dominant plant communities in the basin (see Table 7.4 and Figure 7.5): grassland, mesquite (*Prosopis glandulosa*), creosote (*Larrea tridentata*), tarbush (*Flourensia cernua*), snakeweed (*Xanthocephalum* spp.), other shrubs and no vegetation. Fractional cover for the grassland and snakeweed cover types and plant diameter and height for all vegetation

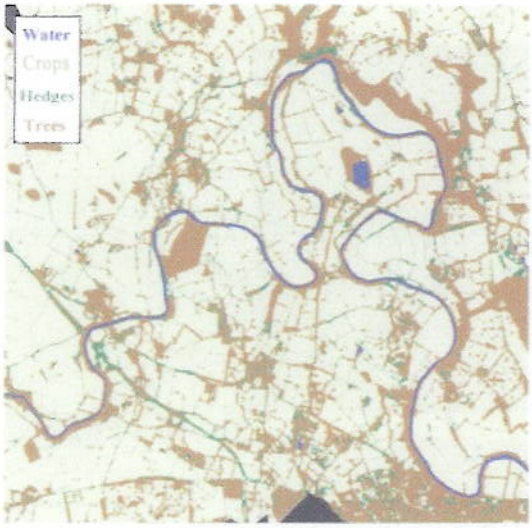

Plate 1 Connected regions identified in the segmentation. Short vegetation is light brown, hedges are green, tall vegetation dark brown and water regions blue

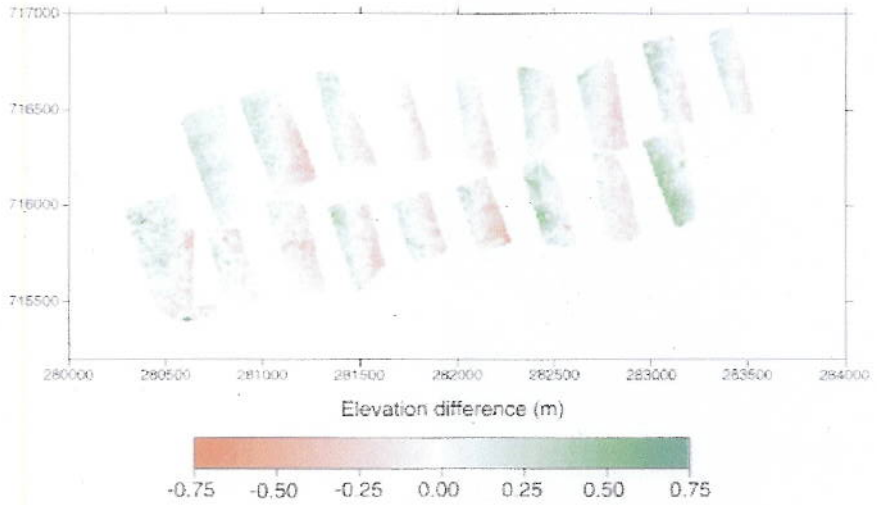

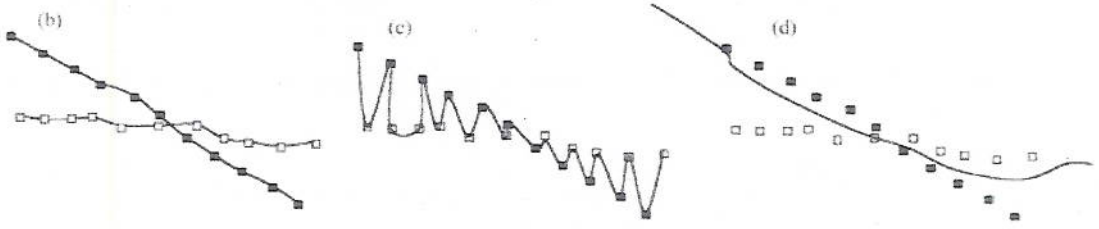

Plate 3 The problem of systematic surface error in areas of DEM overlap. Part (a) shows the results of the DEM overlap; (b) shows this effect in schematic terms; (c) shows the effect of bilinear interpolation as applied to the full dataset without a more sophisticated treatment of overlap areas; and (d) shows DEM combination using distance weighting, considered in section 6.6. Black points are the upstream DEM and white points are the downstream DEM

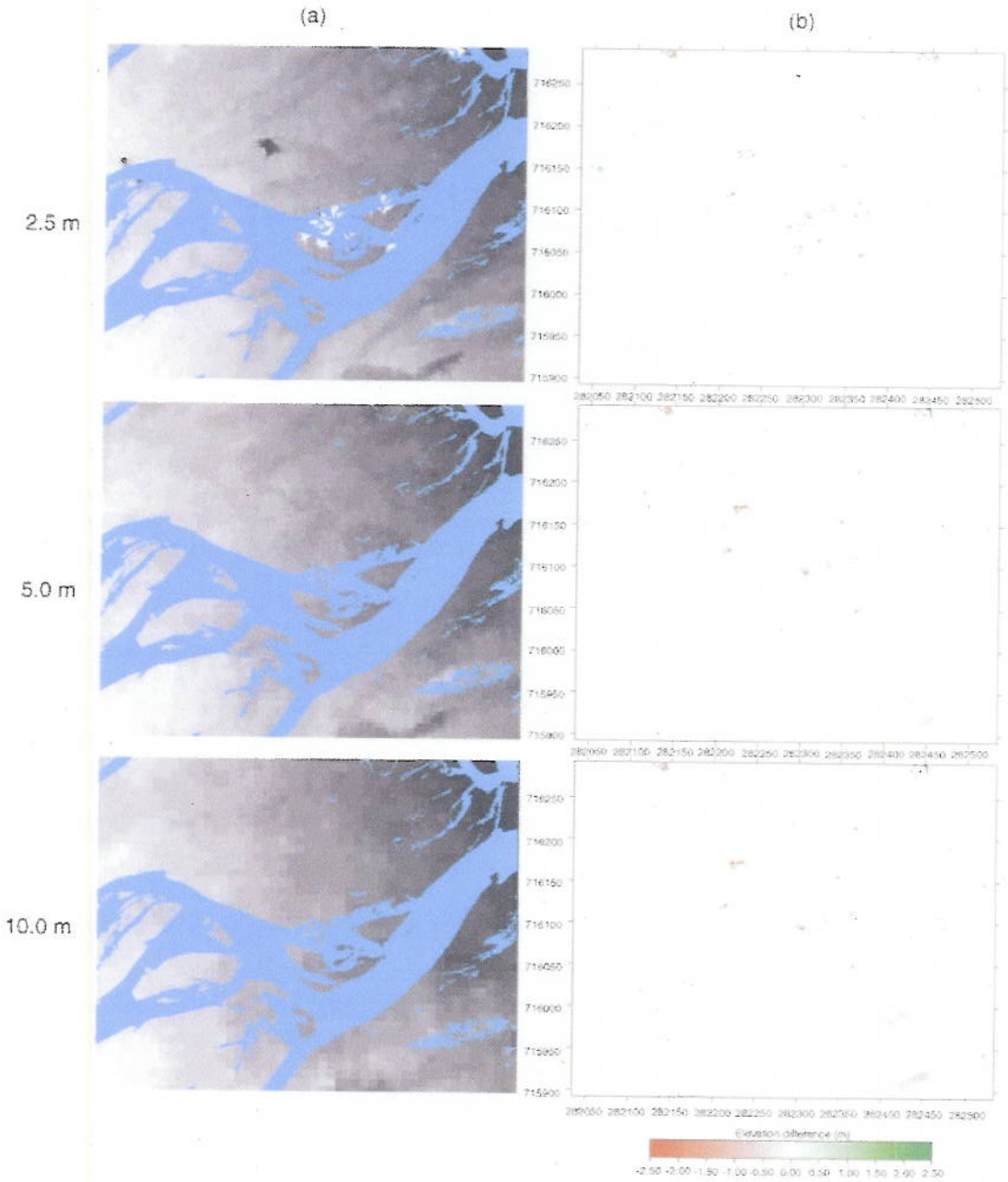

Plate 2 (a) DEMs of the test area collected at three different resolutions and (b) compared with a 1 m DEM

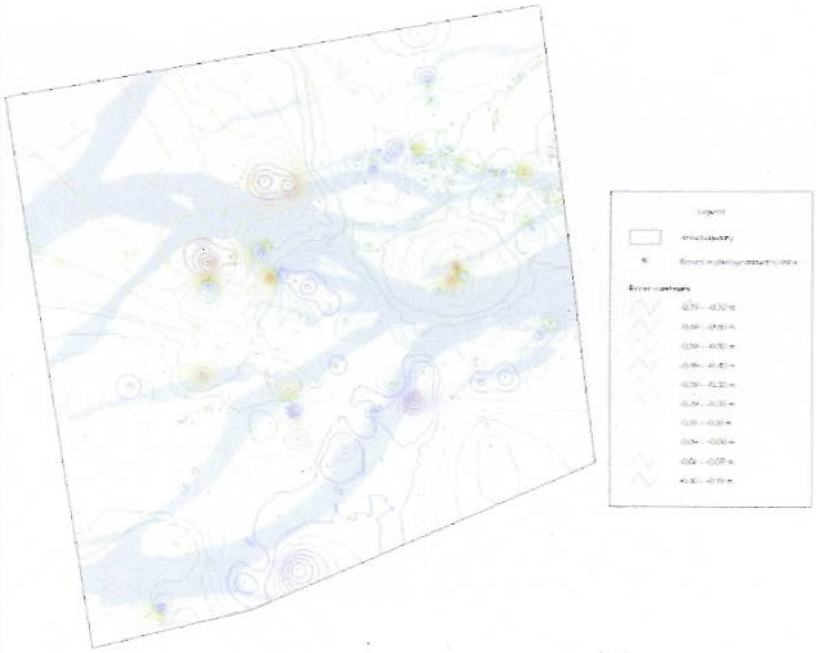

Plate 4 Contoured error surface for an intensively sampled sub-area. It shows that the errors are mainly concentrated around channel margins

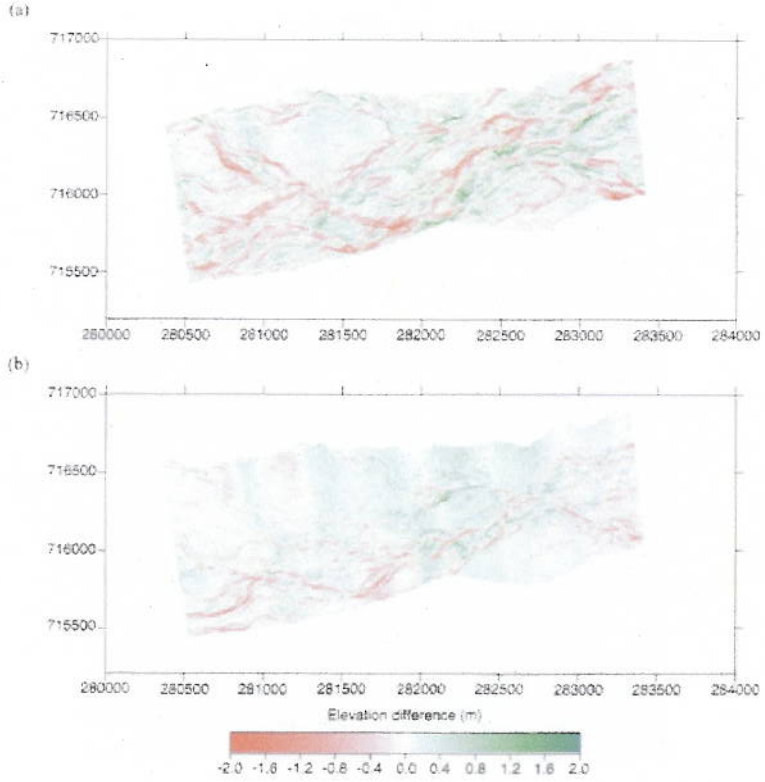

Plate 5 Comparison of the February 1999 DEM with the February 2000 DEM. (a) annual and with the March 1999 DEM (b) storm event, to demonstrate that when erosion and deposition changes are small, the banding effect can still be clearly identified

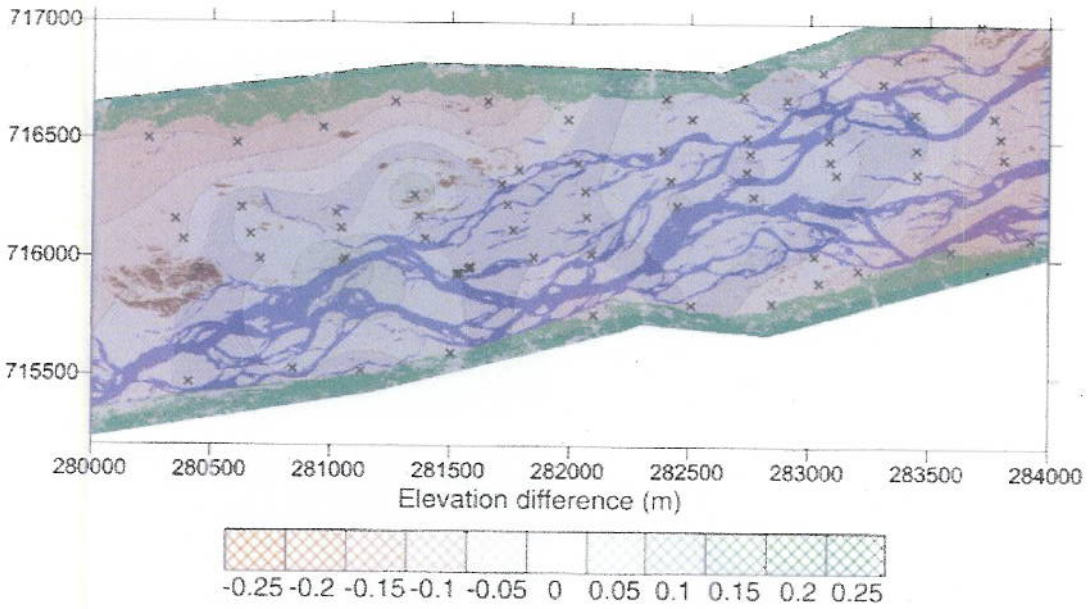

Plate 6 Contoured map of height discrepancies between the post-processed DEM surfaces and ground control point elevations for the February 2000 DEM. Zones of no shading are within ±0.0025 m of surveyed PCP position. The location of individual ground control points is marked

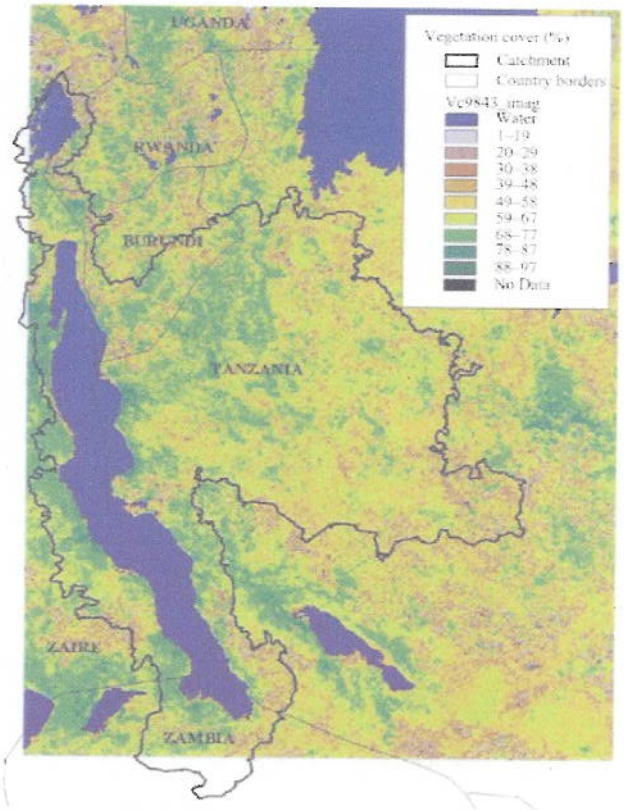

Plate 8 Vegetation cover image (1 km NDVI) for April 1998. Data from the March and May were used to fill the gaps in areas of persistent cloud cover

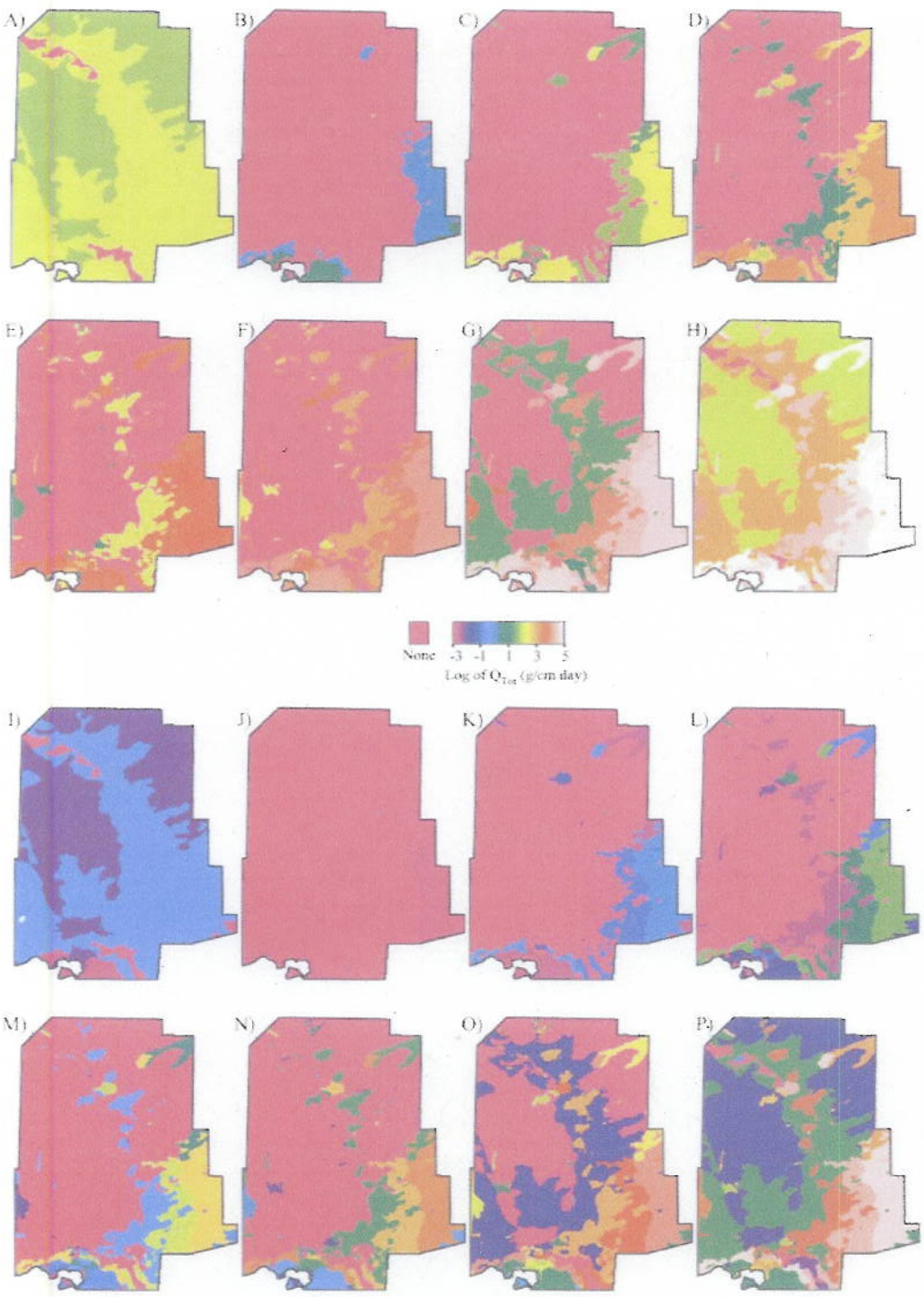

Plate 7 Model estimates of total horizontal flux Q_{Tot} and vertical flux F_a for several scenarios. Wind speeds observed at Jornada, Spring 2000: (a and i) no vegetation (using u_{*_t}); (b and j) vegetation (using u_{*_t}); (c and k) vegetation (using u_{*_t}) using 1.25 × wind speed; (d and l) vegetation (using u_{*_t}) using 1.5 × wind speed; (e and m) vegetation (using u_{*_t}) using 1.75 × wind speed; (f and n) vegetation (using u_{*_t}) using 2.0 × wind speed; (g and o) vegetation (using u_{*_t}) using 2.5 × wind speed; (h and p) vegetation (using u_{*_t}) using 3.0 × wind speed

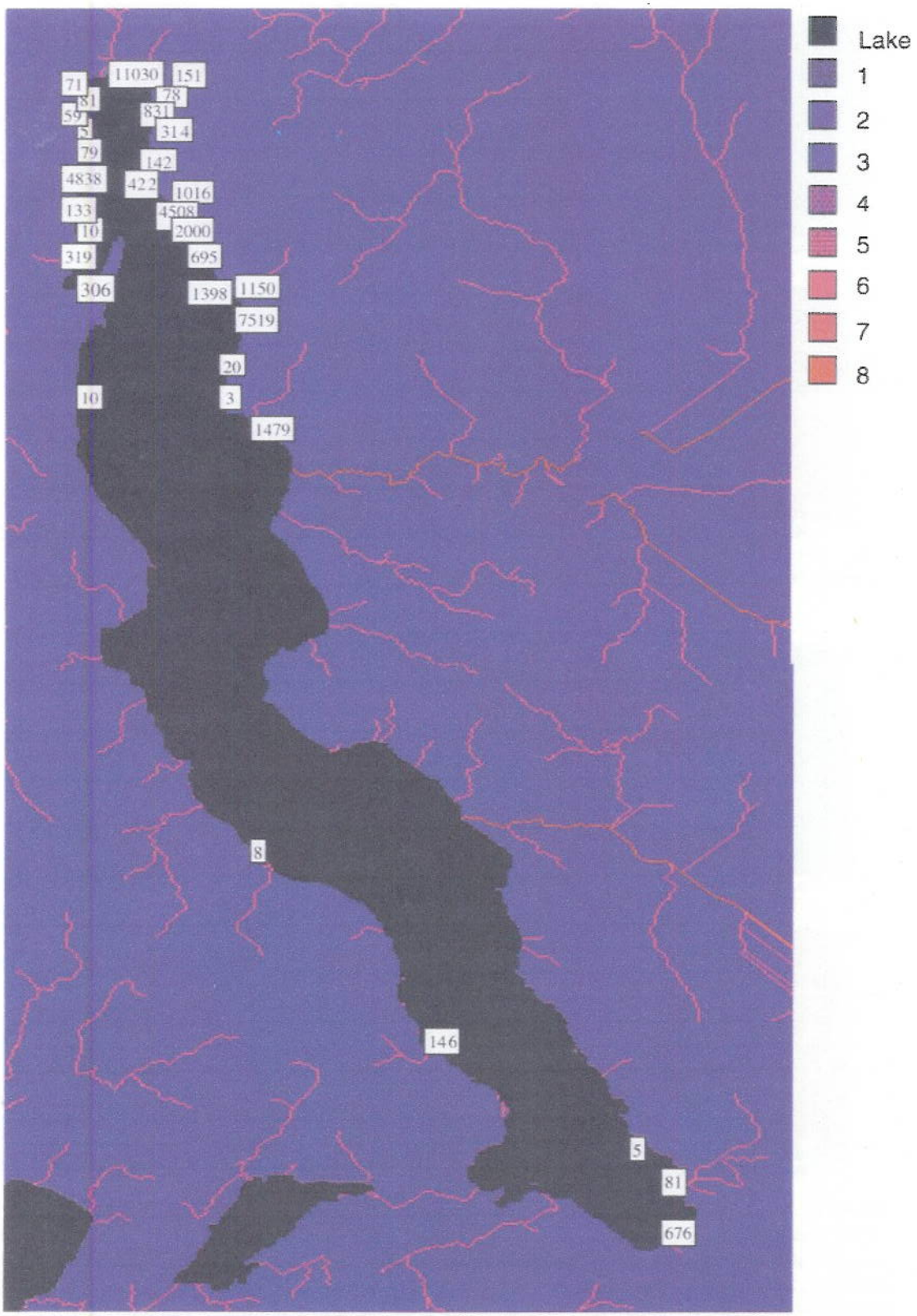

Plate 9 Total sediment yield (tonnes) to Lake Tanganyika recorded in April 1998

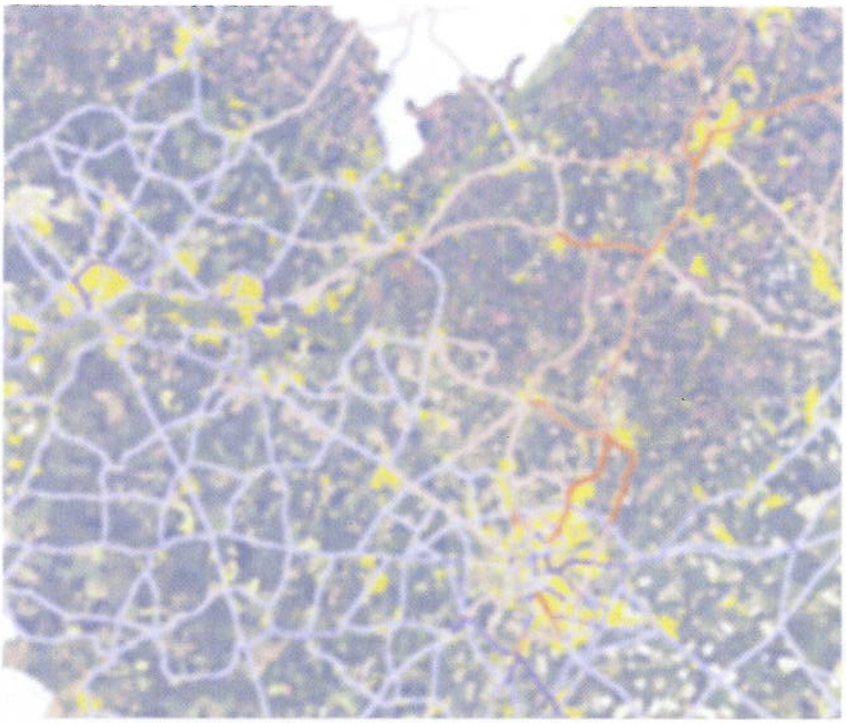

Plate 10 Change in emissions concentrations between the reference scenario and the policy scenario. Dark blue indicates a large decrease in concentration, light blue a small decrease, light pink a small increase and dark pink a large increase. Settlement is picked out in yellow

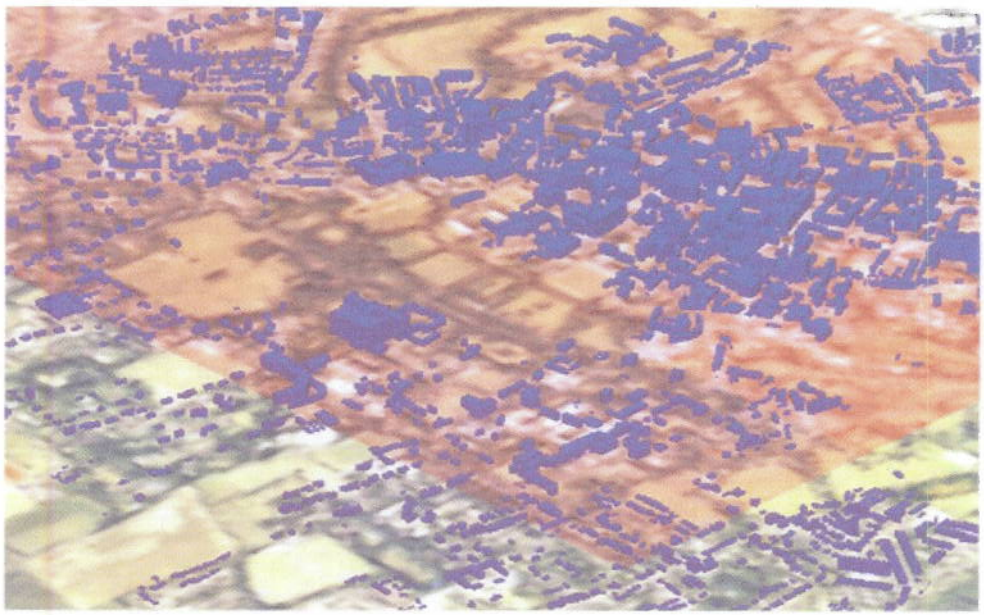

Plate 11 Visualization of emissions concentrations for the Policy Case in West Cambridge. Buildings have been modelled from airborne LiDAR data. Concentration increases with increasing opacity and increasing shades of red

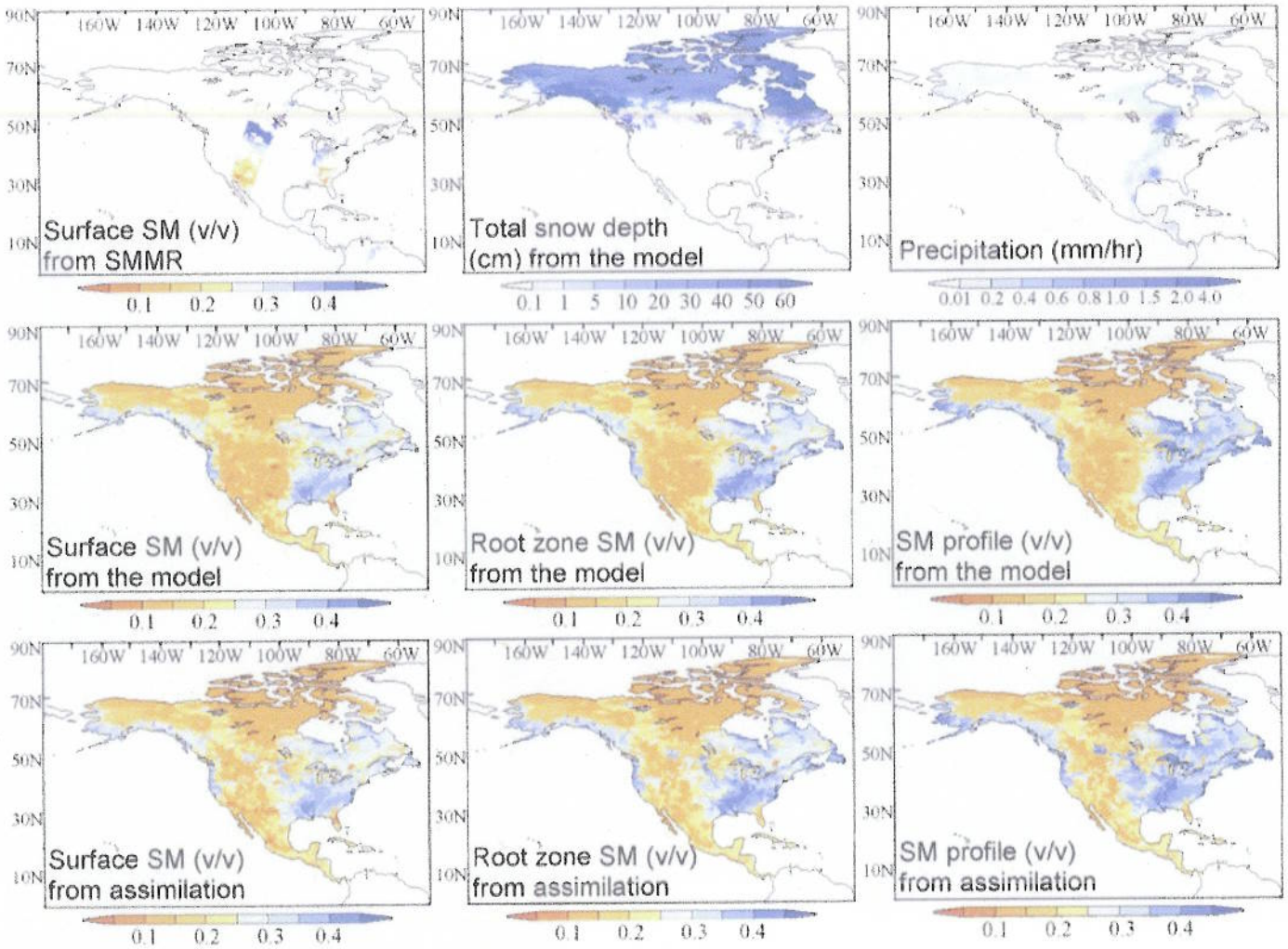

Plate 12 Example of how satellite observations of near-surface soil moisture content may be used to constrain land surface model predictions of soil moisture throughout the soil profile using data assimilation. (Adapted from Walker and Houser 2001)

Table 7.4 SWEMO input parameters for vegetation of the Jornada Basin

Vegetation type	Grass	Mesquite	Creosote	Tarbush	Snakeweed	Other shrubs	Bare
Fractional cover	0.25	0.21	0.17	0.12	0.29	0.17	0.001
Basal area (cm^2)	900	5100	10 800	13 200	100	8500	0.001
Profile area (cm^2)	1000	18 500	9200	13 800	100	8000	0.001
β	100	100	100	100	100	100	1
z_0 (cm)	3.8	4.1	8.2	4.6	1.8	5.6	0.04

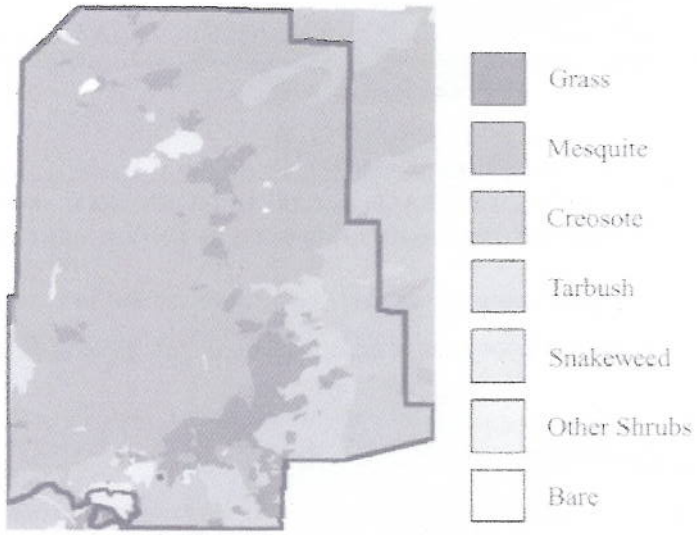

Figure 7.5 Vegetation map of the Jornada Basin derived from mapping efforts at the Jornada Experimental Range and the NMSU College Ranch. The area outlined in black is the region where the soil and vegetation maps overlap and is the study area for the present research

cover types were derived from ongoing vegetation monitoring data as part of the biodiversity Vegetation Transect at Jornada. Fractional cover for the creosote and tarbush cover types was derived from ongoing vegetation monitoring data as part of the Small Mammal Exclosure experiment at Jornada. Fractional cover for the creosote vegetation cover type was taken from Okin and Gillette (2001). Plants were assumed to be cylindrical in shape with basal area equal to π (plant radius)^2 and profile area equal to (plant diameter) (plant height). The drag ratio, β, was taken from Raupach *et al.* (1993) and assumed to be constant for all cover types. Roughness height, z_0, was calculated using equation (4) based on vegetation height, profile area and number density.

Wind Data. Wind monitoring by one of the present authors (Gillette) has been ongoing at several sites in the Jornada for many years. Data from one windy season (28 March 2000–10 July 2000) was used in this study (Figure 7.6). Although wind direction was also

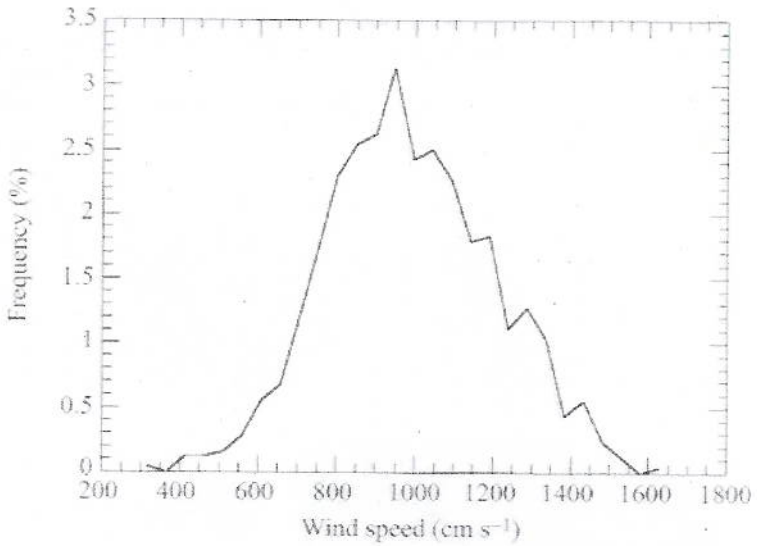

Figure 7.6 *Frequency of wind speeds at one monitoring site at Jornada. Measurements were taken at 1490 cm from the period 28 March 2000 to 10 July 2000. Wind speeds below 300 cm s^{-1} were not recorded. Frequency is reported as percent of entire 105-day wind record*

recorded, direction is assumed not to have an impact on the magnitude of wind erosion and dust flux.

7.5.2 Running the Model

SWEMO uses soil texture and vegetation maps as its primary inputs, and from these produces intermediate maps of parameters required for evaluating the equations (1) and (2). Thus, the first step in generating spatially explicit estimates of wind erosion and dust flux, is the production of these intermediate products (Figures 7.7–7.10). Figures 7.7–7.9 are generated in a straightforward way by determining vegetation type or soil texture in each model cell and then looking up the appropriate value of u_{*ts}, z_0 or k from associated look-up table files (see Tables 7.3 and 7.4). Figure 7.10 is generated by determining vegetation type and soil texture for each model cell, looking up values of u_{*ts} as well as plant structural parameters in the associated look-up table files and evaluating equation (7) for each cell.

A record of wind speed is imported into the model and compressed by creating a histogram of the data. This histogram is then used to calculate a histogram of u_* using equation (2) and values of z_0 for each cell (Figure 7.8). The histogram approach to working with wind speed data is the most computationally efficient way to evaluate equation (1) for each cell, because it allows estimation of horizontal flux for a few wind speed bins, as opposed to each entry in an entire wind speed record.

Once the intermediate maps and u_* histograms have been created, equation (1) is evaluated for each cell to generate estimates of Q_{Tot} for each cell. Data from Figure 7.9 are then used to convert the Q_{Tot} map into maps of dust flux, F_a.

In the present research, Q_{Tot} and F_a were evaluated for the entire study area for eight scenarios:

Figure 7.7 Map of the threshold shear velocity for unvegetated soil, u_{*ts}, derived from the soil texture map and literature values for u_{*ts}

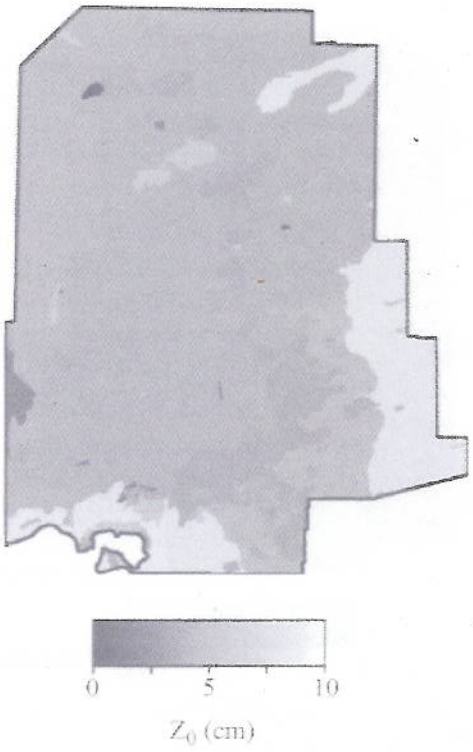

Figure 7.8 Map of the roughness height, z_0, derived by evaluating equation (4) for each vegetation height based on its measured height (see Table 7.4)

Figure 7.9 *Map of the ratio of vertical flux to horizontal flux, F_a/Q_{Tot}, derived from the soil texture map and literature values*

Figure 7.10 *Map of the threshold shear velocity for vegetated soil, u_{*t}, derived by evaluating equation (7) for the entire study area*

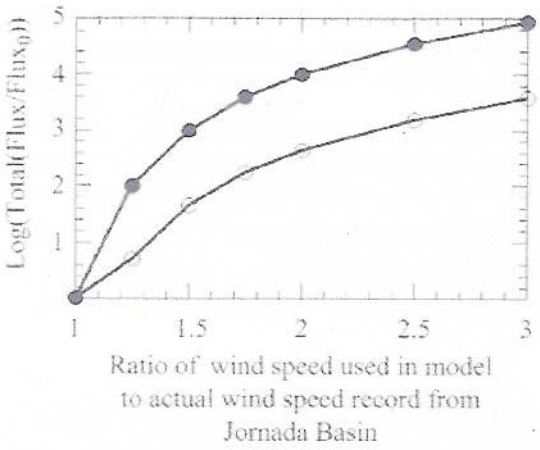

Figure 7.11 *Log of total flux with elevated wind speed divided by total flux with measured wind speed. Flux is either Q_{Tot} or F_a for elevated wind speed. Flux$_0$ is either Q_{Tot} and F_a for measured wind speed. Results for Q_{Tot} are shown by close circles and results for F_a are shown by open circles*

1. No vegetation, wind record from Jornada (Plates 7(a) and 7(i))
2. Mapped vegetation (Figure 7.5), wind speed record from Jornada (Plates 7(b) and 7(j); wind speed record shown in Figure 7.6)
3. Mapped vegetation, Jornada wind speed record multiplied by 1.25 (Plates 7(c) and 7(k))
4. Mapped vegetation, Jornada wind speed record multiplied by 1.5 (Plates 7(d) and 7(l))
5. Mapped vegetation, Jornada wind speed record multiplied by 1.75 (Plates 7(e) and 7(m))
6. Mapped vegetation, Jornada wind speed record multiplied by 2.0 (Plates 7(f) and 7(n))
7. Mapped vegetation, Jornada wind speed record multiplied by 2.5 (Plates 7(g) and 7(o))
8. Mapped vegetation, Jornada wind speed record multiplied by 3.0 (Plates 7(h) and 7(p))

By increasing the wind speeds used in the model over the measured wind speeds at Jornada, we were able to evaluate the effect that windier conditions would have at the site. Calculating the total of Q_{Tot} and F_a for the entire area, the overall effect of increased wind speed for the area was evaluated (Figure 7.13).

7.5.3 Discussion of Model Results

Values of Q_{Tot} for the study area (Plate 7) compare favourably with measured values of dust flux in several cover types within the Basin for a period encompassing the period of the wind record (Table 7.5). However, the model predicts no wind erosion or dust flux for much of the Basin, most notably the mesquite areas which display the highest measured

Table 7.5 *Summary of measured values of Q_{Tot} for different vegetation types in the Jornada Basin for the period 24 July 1998 to 19 April 2001.*

	$\text{Log}(Q_{Tot}(\text{g cm}^{-1}/\text{day}))$					
Vegetation type	Grassland	Mesquite	Creosote	Tarbush	Playa	Bare
Average	−1.1	0.0	−1.0	−1.0	−0.8	1.5
Minimum	−3.0	−0.6	−3.0	−2.3	−1.9	0.7
Maximum	−0.3	0.9	−0.2	−0.4	−0.3	2.3

Figure 7.12 *Oblique aerial photograph taken in 1975 during a dust storm in West Texas, USA. Notice that plumes are formed over a small fraction of the total amount of agricultural land (from Gillette (1999), reproduced with permission)*

dust flux among vegetated surfaces. This effect is largely due to the high-threshold shear velocity calculated for combinations of vegetation and soil (Figure 7.7) and as a result, the area of no modelled wind erosion is seen to dwindle with increasing wind speed (Plate 7).

Gillette (1999) has suggested that the bulk of wind erosion and dust flux that occurs often occurs as small 'hot spots' within the landscape (Figure 7.12). These areas may be roads, small disturbance, or as Okin and Gillette (2001) have pointed out, self-organizing 'streets' in the landscape. Streets are elongated unvegetated areas, usually aligned with the wind, down which wind blows, thus effectively reducing u_{*t} over small scales. Okin and Gillette have suggested that these streets may be responsible for the observed high-flux rates in mesquite dunelands. SWEMO assumes homogenous vegetation cover and distribution within each vegetation type. Thus, our results suggest that the assumption of homogenous vegetation cover is not adequate for spatial modelling of wind erosion. More complicated models that incorporate these erosion hot spots are required to reproduce vegetation with high fidelity.

Despite this, the modelled increase in Q_{Tot} and F_a with increasing wind speed confirms the predictions of Gregory *et al.* (1999) that wind erosion and dust flux increase non-linearly with increasing wind speed. As Plate 7 shows, this effect is the result of two factors: (1) increased number of areas subject to wind erosion (areas with $u_* > u_{*t}$); and (2) increased flux from areas undergoing wind erosion (increased $u_*^2 - u_{*t}^2$). Because wind erosion is controlled in large part by the difference between u_* and u_{*t} for conditions where $u_* > u_{*t}$, and u_{*t} is largely controlled by variable vegetation cover (equation (7)), evaluating Q_{Tot} and F_a for elevated wind speeds also serves as a proxy for conditions when vegetation cover may be decreased due to low vegetation conditions, due, say, to drought.

7.6 Conclusion

The mismatch between observed patterns of wind erosion and dust flux and the patterns modelled using SWEMO most likely arises from the fact that in natural environments, small wind erosion hot spots are responsible for the vast majority of flux. New modelling techniques need to be developed which can incorporate these small-scale spatial phenomena into large-scale dust flux models. In addition, new techniques must be developed which can identify, quantify and map these erosion hot spots in the landscape.

A potential method to map hot spots, in addition to providing more detailed information about surface properties, is to derive estimates of the relevant parameters from remote sensing data. Some attempt has been made to do this in previous studies, although not for the original purposes of wind erosion modelling. Okin *et al.* (2001c) and Okin and Gillette (2001), for example, have derived estimates of surface cover in areas susceptible to wind erosion using spectral mixture analysis and geostatistics of aerial photographs, respectively. Other authors have tried to develop remote sensing tools that estimate vegetation number density and size using the Li-Strahler optical canopy model (see, for example, Li and Strahler, 1985; Franklin and Strahler, 1988; Li and Strahler, 1992; Scarth and Phinn, 2000).

Spatial modelling of wind erosion remains in its infancy. Because large-scale dust emission often depends on very small-scale heterogeneities on the land surface, the SWEMO model described here is only a first step in developing a full modelling approach to this fundamental geomorphological process that dominates the world's arid and semi-arid regions – 30% of the Earth's land surface.

Acknowledgements

Data was provided for this work by NSF grant DEB 00-84012 as a contribution to the Jornada (LTER) programme.

References

Alward, R.D., Detling, J.K. and Milchunas, D.G., 1999, Grassland vegetation changes and nocturnal global warming, *Science*, **283**, 229–231.

Bagnold, R.A., 1941, *The Physics of Blown Sand and Desert Dunes* (New York: Methuen).

Bahre, C.J., 1991, *A Legacy of Change: Historic Human Impact on Vegetation in the Arizona Borderlands* (Tucson, Arizona: University of Arizona Press).

Bahre, C.J. and Shelton, M.L., 1993, Historic vegetation change, mesquite increases and climate in southeastern Arizona, *Journal of Biogeography*, **20**, 489–514.

Brown, J.H., Valone, T.J. and Curtin, C.G., 1997, Reorganization of an arid ecosystem in response to recent climate change, *Proceedings of the National Academy of Science of the United States of America*, **94**, 9729–9733.

Buffington, L.C. and Herbel, C.H., 1965, Vegetational changes on a semidesert grassland range from 1858 to 1963, *Ecological Monograph*, **35**, 139–164.

Chadwick, O.A., Derry, L.A., Vitousek, P.M., Huebert, B.J. and Hedin, L.O., 1999, Changing sources of nutrients during four million years of ecosystem development, *Nature*, **397**, 491–497.

Coale, K.H., Johnson, K.S., Fitzwater, S.E., Gordon, R.M., Tanner, S., Chavez, F.P., Ferioli, L., Sakamoto, C., Rogers, P., Millero, F., Steinberg, P., Nightingale, P., Cooper, D., Cochlan, W.P., Landry, M.R., Constantinou, J., Rollwagen, G., Trasvina, A. and Kudela, R., 1996, A massive phytoplankton bloom induced by an ecosystem-scale iron fertilization experiment in the equatorial Pacific Ocean, *Nature*, **383**, 495–501.

Dentener, F.J., Carmichael, G.R., Zhang, Y., Lelieveld, J. and Crutzen, P.J., 1996, Role of mineral aerosol as a reactive surface in the global troposphere, *Journal of Geophysical Research-Atmospheres*, **101**, 22869–22889.

Dickerson, R.R., Kondragunta, S., Stenchikov, G., Civerolo, K.L., Doddridge, B.G. and Holben, B.N., 1997, The impact of aerosols on solar ultraviolet radiation and photochemical smog, *Science*, **278**, 827–830.

Duce, R.A. and Tindale, N.W., 1991, Atmospheric transport of iron and its deposition in the ocean, *Limnology and Oceanography*, **36**, 1715–1726.

Forman, S.L., Goetz, A.F.H. and Yuhas, R.H., 1992, Large-scale stabilized dunes on the high plains of Colorado: understanding the landscape response to Holocene climates with the aid of images from space, *Geology*, **20**, 145–148.

Franklin, J. and Strahler, A.H., 1988, Invertible canopy reflectance modelling of vegetation structure in semiarid woodland, *IEEE Transactions on Geoscience and Remote Sensing*, **26**, 809–825.

Gillette, D.A., 1988, Threshold friction velocities for dust production for agricultural soils, *Journal of Geophysical Research*, **93**, 12645–12662.

Gillette, D.A., 1999, A qualitative geophysical explanation for 'hot spot' dust emission source regions, *Contributions to Atmospheric Physic*, **72**, 67–77.

Gillette, D.A. and Chen, W.A., 2001, Particle production and aeolian transport from a 'supply-limited' source area in the Chihuahuan desert, New Mexico, United States, *Journal of Geophysical Research*, **106**, 5267–5278.

Gillette, D.A., Fryrear, D.W., Gill, T.E., Ley, T., Cahill, T.A. and Gearhart, E.A., 1997, Relation of vertical flux of particles smaller than 10 μm to aeolian horizontal mass flux at Owens Lake, *Journal of Geophysical Research*, **102**, 26009–26015.

Ginoux, P., Chin, M., Tegen, I., Prospero, J.M., Holben, B., Dubovik, O. and Lin, S.J., 2001, Sources and distributions of dust aerosols simulated with the GOCART model, *Journal of Geophysical Research-Atmospheres*, **106**, 20255–20273.

Gregory, P.J., Ingram, J.S.I., Campbell, B., Goudriaan, J., Hunt, L.A., Landsberg, J.J., Linder, S., Stafford Smith, M. and Sutherst, R.W., 1999, Managed production systems, in B. Walker, W. Steffen, J. Canadell, and J. Ingram (eds), *The Terrestrial Biosphere and Global Change: Implications for Natural and Managed Ecosystems*, Vol. 4 (Cambridge: Cambridge University Press), 229–270.

Griffin, D.W., Garrison, V.H., Herman, J.R. and Shinn, E.A., 2001, African desert dust in the Caribbean atmosphere: microbiology and public health, *Aerobiologia*, **17**, 203–213.

Guelle, W., Balkanski, Y.J., Schulz, M., Marticorena, B., Bergametti, G., Moulin, C., Arimoto, R. and Perry, K.D., 2000, Modeling the atmospheric distribution of mineral aerosol: comparison with ground measurements and satellite observations for yearly and synoptic timescales over the North Atlantic, *Journal of Geophysical Research-Atmospheres*, **105**, 1997–2012.

Kaimal, J.C. and Finnigan, J.J., 1994, *Atmospheric Boundary Layer Flows* (Oxford: Oxford University press).

Lancaster, N. and Baas, A., 1998, Influence of vegetation cover on sand transportation by wind: field studies at Owens Lake, California, *Earth Surface Processes and Landforms*, **23**, 69–82.

Lettau, H.H., 1969, Note on aerodynamic roughness-parameter estimation on the basis of roughness element description, *Journal of Applied Meteorology*, **8**, 828–832.

Levin, Z., Ganor, E. and Gladstein, V., 1996, The effects of desert particles coated with sulfate on rain formation in the eastern Mediterranean, *Journal of Applied Meteorology*, **35**, 1511–1523.

Li, X. and Strahler, A.H., 1985, Geometric-optical modelling of a conifer forest, *IEEE Transactions on Geoscience and Remote Sensing*, **23**, 705–721.

Li, X. and Strahler, A.H., 1992, Geometric-optical bidirectional reflectance modelling of the discrete crown vegetation canopy: effect of crown shape and mutual shadowing, *IEEE Transactions on Geoscience and Remote Sensing*, **30**, 276–291.

Mahowald, N.M., Zender, C., Luo, C. and del Corral, J. (submitted), Understanding the 30-year Barbados desert dust record, *Journal of Geophysical Research*.

Marticorena, B., Bergametti, G., Aumont, B., Callot, Y., N'Doumé, C. and Legrand, M., 1997, Modeling the atmospheric dust cycle: 2. Simulation of Saharan sources, *Journal of Geophysical Research*, **102**, 4387–4404.

Okin, G.S. and Gillette, D.A., 2001, Distribution of vegetation in wind-dominated landscapes: implications for wind erosion modelling and landscape processes, *Journal of Geophysical Research*, **106**, 9673–9683.

Okin, G.S., Murray, B. and Schlesinger, W.H., 2001a, Degradation of sandy arid shrubland environments: observations, process modelling and management implications, *Journal of Arid Environments*, **47**, 123–144.

Okin, G.S., Murray, B. and Schlesinger, W.H., 2001b, Desertification in an arid shrubland in the southwestern United States: process modeling and validation, in A. Conacher (ed.), *Land Degradation: Papers Selected from Contributions to the Sixth Meeting of the International Geographical Union's Commission on Land Degradation and Desertification, Perth, Western Australia, 20–28 September 1999* (Dordrecht: Kluwer Academic Publishers), 53–70.

Okin, G.S., Okin, W.J., Murray, B. and Roberts, D.A., 2001c, Practical limits on hyperspectral vegetation discrimination in arid and semiarid environments, *Remote Sensing of Environment*, **77**, 212–225.

Owen, P.R., 1964, Saltation of uniform grains in air, *Journal of Fluid Mechanics*, **20**, 225–242.

Paulsen, H.A., Jr. and Ares, F.N., 1962, Grazing values and management of black gramma and tobosa grasslands and associated shrub ranges of the Southwest, *U.S. Forest Service*.

Piketh, S.J., Tyson, P.D. and Steffen, W., 2000, Aeolian transport from southern Africa and iron fertilization of marine biota in the South Indian Ocean, *South African Journal of Geology*, **96**, 244–246.

Prospero, J.M., Ginoux, P., Torres, O. and Nicholson, S.E. (2002), Environmental characterization of global sources of atmospheric soil dust derived from the NIMBUS-7 absorbing aerosol product, *Reviews of Geophysics*, **40**, 2.1–2.31.

Raupach, M.R., Gillette, D.A. and Leys, J.F., 1993, The effect of roughness elements on wind erosion threshold, *Journal of Geophysical Research*, **98**, 3023–3029.

Reynolds, R., Belnap, J., Reheis, M., Lamothe, P. and Luiszer, F., 2001, Aeolian dust in Colorado Plateau soils: nutrient inputs and recent change in source, *Proceedings of the National Academy of Sciences of the United States of America*, **98**, 7123–7127.

Rosenzweig, C. and Hillel, D., 1993, The dust bowl of the 1930s: analog of greenhouse effect in the Great Plains, *Journal of Environmental Quality*, **22**, 9–22.

Scarth, P. and Phinn, S., 2000, Determining forest structural attributes using an inverted geometric-optical model in mixed eucalypt forests, Southeast Queensland, Australia, *Remote Sensing of Environment*, **71**, 141–157.

Schlesinger, W.H., Reynolds, J.F., Cunningham, G.L., Huenneke, L.F., Jarrell, W.M., Virginia, R.A. and Whitford, W.G., 1990, Biological feedbacks in global desertification, *Science*, **247**, 1043–1048.

Schultz, B.W. and Ostler, W.K., 1993, Effects of prolonged drought on vegetation association in the Northern Mojave Desert, *Wildland Shrubs and Arid Land Restoration Symposium*, Las Vegas, Nevada, 228–235.

Shao, Y. and Raupach, M.R., 1993, Effect of saltation bombardment on the entrainment of dust by wind, *Journal of Geophysical Research*, **98**, 12719–12726.

Soil Conservation Service, 1980, *Soil Survey of Doña Ana County, New Mexico* (United States Department of Agriculture, Soil Conservation Service).

Sokolik, I.N. and Toon, O.B., 1996, Direct radiative forcing by anthropogenic airborne mineral aerosols, *Nature*, **381**, 681–683.

Stockton, P.H. and Gillette, D.A., 1990, Field measurement of the sheltering effect of vegetation on erodible land surfaces, *Land Degradation and Rehabilitation*, **2**, 77–85.

Tegen, I. and Fung, I., 1995, Contribution to the atmospheric mineral aerosol load from land surface modification, *Journal of Geophysical Research*, **100**, 18707–18726.

Tegen, I. and Lacis, A.A., 1996, Modeling of particle size distribution and its influence on the radiative properties of mineral dust aerosol, *Journal of Geophysical Research*, **101**, 19237–19244.

Wooding, R.A., Bradley, E.F. and Marshall, J.K., 1973, Drag due to regular arrays of roughness elements of varying geometry, *Boundary-Layer Meteorology*, **5**, 285–308.

Wurzler, S., Reisin, T.G. and Levin, Z., 2000, Modification of mineral dust particles by cloud processing and subsequent effects on drop size distributions, *Journal of Geophysical Research*, **105**, 4501–4512.